

Domain organization and structure–function relationship of the HET-s prion protein of *Podospora anserina*

Axelle Balguerie, Suzana Dos Reis, Christiane Ritter¹, Stéphane Chaignepain², Bénédicte Couлары-Salin³, Vincent Forge⁴, Katell Bathany², Ioan Lascu⁵, Jean-Marie Schmitter², Roland Riek¹ and Sven J.Saupe⁶

Laboratoire de Génétique Moléculaire des Champignons, ³Service de Microscopie and ⁵Laboratoire d'Enzymologie Moléculaire, Institut de Biochimie et de Génétique Cellulaires, UMR 5095 CNRS/Université de Bordeaux 2, 1 rue Camille St Saëns, 33077 Bordeaux cedex, ²Institut Européen de Chimie et Biologie, CNRS FRE 2247, 16 Av. Pey Berland, 33607 Pessac cedex, ⁴Laboratoire de Biophysique Moléculaire et Cellulaire, UMR 5090, Département de Biologie Moléculaire et Structurale, CEA-Grenoble, 17 rue de Martyrs, 38054 Grenoble cedex 9, France and ¹Structural Biology Laboratory, The Salk Institute for Biological Studies, PO Box 85800, San Diego, CA 92186-5800, USA

⁶Corresponding author
e-mail: sven.saupe@ibgc.u-bordeaux2.fr

A.Balguerie and S.Dos Reis contributed equally to this work

The [Het-s] infectious element of the fungus *Podospora anserina* is a prion protein involved in a genetically controlled cell death reaction termed heterokaryon incompatibility. Previous analyses indicate that [Het-s] propagates as a self-perpetuating amyloid aggregate. The HET-s protein is 289 amino acids in length. Herein, we identify the region of the HET-s protein that is responsible for amyloid formation and prion propagation. The region of HET-s spanning residues 218–289 forms amyloid fibers *in vitro* and allows prion propagation *in vivo*. Conversely, a C-terminal deletion in HET-s prevents amyloid aggregation *in vitro* and prion propagation *in vivo*, and abolishes the incompatibility function. In the soluble form of HET-s, the region from residue 1 to 227 forms a well-folded domain while the C-terminal region is highly flexible. Together, our data establish a domain structure–function relationship for HET-s amyloid formation, prion propagation and incompatibility activity.

Keywords: amyloid/filamentous fungi/heterokaryon incompatibility/prion

Introduction

Prions are infectious proteins that propagate an altered conformational state. The mammalian PrP prion protein is responsible for a class of fatal neurological diseases termed transmissible spongiform encephalopathies (Prusiner, 1998). Prions have also been identified in yeast and in the fungus *Podospora anserina* as genetic elements displaying non-mendelian inheritance (Wickner,

1994; Coustou *et al.*, 1997). These fungal prion models have proven valuable to gain insight into the mechanism of prion propagation. Like PrP, yeast and fungal prion proteins form amyloid fibers *in vitro* (Glover *et al.*, 1997; King *et al.*, 1997; Taylor *et al.*, 1999; Dos Reis *et al.*, 2002). Amyloids are fibrillar aggregates that are characterized by a cross- β structure and an increased resistance to proteolysis. This type of protein aggregate is associated not only with prion diseases but also with a large group of protein deposition diseases including Alzheimer's, Parkinson's and Huntington's diseases (Koo *et al.*, 1999). Amyloids can be formed from proteins that adopt an unordered conformation in native conditions (so-called 'natively unfolded' proteins) or from globular proteins exposed to mildly denaturing conditions. It thus appears that amyloid formation involves unordered or at least partly unfolded precursors (Dobson, 1999).

The [Het-s] prion of the fungus *Podospora anserina* is involved in a genetically controlled programmed cell death phenomenon termed heterokaryon incompatibility (Glass *et al.*, 2000; Saupe, 2000). This cell death reaction occurs when cells of unlike genotype fuse. The *het-s* locus has two antagonistic alleles termed *het-s* and *het-S*. The *het-s*- and *het-S*-encoded proteins differ by 13 amino acid residues (Turcq *et al.*, 1991) (Figure 1). The HET-s protein (unlike HET-S) can undergo a transition from a normal to an infectious prion state (Coustou *et al.*, 1997). Strains expressing the HET-s protein thus exist as two alternative states, the active [Het-s] prion-infected state and the neutral [Het-s*] state. When a [Het-s] strain fuses with a *het-S* strain, the fusion cell dies. Conversely, the fusion of a prion-free [Het-s*] with *het-S* leads to the formation of a viable mixed cell (heterokaryon). [Het-s] can infect a [Het-s*] strain by simple contact, and the [Het-s] prion propagates in the mycelium at a rate of up to 70 mm per day. *In vivo*, a HET-s–green fluorescent protein (GFP) fusion protein undergoes a transition from a soluble to an aggregated state upon transition to the prion state, thus suggesting that [Het-s] propagates as a self-perpetuating HET-s aggregate (Coustou-Linares *et al.*, 2001). Recombinant full-length HET-s forms amyloid aggregates *in vitro* (Dos Reis *et al.*, 2002). Transition from the soluble to the aggregated state is accompanied by an increase in β -sheet content and the formation of a 7 kDa protease-resistant fragment (Dos Reis *et al.*, 2002). Amyloid aggregates of recombinant HET-s are able to induce the [Het-s] prion form when introduced by a biolistic procedure into prion-free [Het-s*] strains (Maddelein *et al.*, 2002). Soluble HET-s or amorphous aggregates of HET-s display no infectivity in this assay. The 7 kDa protease-resistant fragment maintains its fibrillar state and displays infectivity in the biolistic assay (Maddelein *et al.*, 2002).

These results suggested that the prion properties of HET-s could be due to a limited region of the protein. In

Table I. Prion propagation activity and incompatibility phenotype of *het-s* transformants

Construct	Background	GFP signal	[Het-s] propagation	Incompatibility phenotype
Vector	<i>het-s</i>	–	+	[Het-s]
Vector	Δ <i>het-s</i>	–	–	Null
HET-s	Δ <i>het-s</i>	–	+	[Het-s]
HET-S	Δ <i>het-s</i>	–	–	[Het-S]
218–289	<i>het-s</i>	–	+	[Het-s]
218–289	Δ <i>het-s</i>	–	–	Null
218–289–GFP	<i>het-s</i>	Aggregated	+	[Het-s]
218–289–GFP	Δ <i>het-s</i>	Diffuse/Aggregated ^a	+	[Het-s]
1–227	<i>het-s</i>	–	+	[Het-s]
1–227	Δ <i>het-s</i>	–	–	Null
1–227–GFP	<i>het-s</i>	Diffuse	+	[Het-s]
1–227–GFP	Δ <i>het-s</i>	Diffuse	–	Null
1–240	Δ <i>het-s</i>	–	–	Null
1–240–GFP	Δ <i>het-s</i>	Diffuse	–	Null
HET-S 1–227	Δ <i>het-s</i>	–	–	Null
HET-S 1–227	<i>het-s</i>	–	+	[Het-s]
HET-sS	Δ <i>het-s</i>	–	+	[Het-s]
HET-Ss	Δ <i>het-s</i>	–	–	[Het-S]
GPD-HET-sS ^b	Δ <i>het-s</i>	–	+	[Het-s]
GPD-HET-Ss ^b	Δ <i>het-s</i>	–	–	[Het-S]

^aGFP distribution switched from diffuse to aggregated after contact with a wild-type [Het-s] strain.

^bChimeric proteins expressed under control of the strong GPD promoter.

Table II. MALDI mass spectrometry of HET-s proteolytic digestion products

HET-s form	Proteolysis	Stretch	Calculated mass	Measured mass	PSD sequence ions ^c
Soluble	Proteinase K	2–240	26 749.5 ^a	26 740 ^a	
Soluble	Proteinase K	10–240	25 948.5 ^a	25 950 ^a	
Soluble	Proteinase K + AspN	230–240	1372.73 ^b	1372.74 ^b	b ₇ –b ₁₀ , y ₆ –y ₁₀
Aggregated	Proteinase K + LysC	218–229	1271.74 ^b	1272.76 ^b	
Aggregated	Proteinase K + LysC	219–229	1143.65 ^b	1143.71 ^b	
Aggregated	Proteinase K + LysC	230–270	4363.88 ^a	4363.79 ^a	
Aggregated	Proteinase K + LysC	271–284	1478.76 ^b	1478.81 ^b	
Aggregated	Proteinase K + LysC	285–295	1460.61 ^b	1460.78 ^b	b ₆ –b ₁₀ , y ₁ –y ₄

^aAverage masses for [M + H]⁺ ions.

^bMonoisotopic masses for [M + H]⁺ ions.

^cAccording to the nomenclature proposed by Roepstorff and Fohlman (1984).

At equivalent molar concentrations, aggregation of HET-s(218–289) is about two orders of magnitude faster than aggregation of full-length HET-s (Figure 4A) (Dos Reis *et al.*, 2002). HET-s(218–289) aggregates efficiently catalyze aggregation of full-length HET-s (Figure 4B).

To measure the conformation of HET-s(218–289), the circular dichroism (CD) spectrum of purified HET-s(218–289) was measured immediately after increasing the pH from 2.5 to 8.0. The spectrum displays a strong negative signal at ~198 nm characteristic of random coil secondary structure (Figure 5A). In contrast, the CD spectrum of aggregated HET-s(218–289) displays a minimum at ~218 nm and a positive band at 196 nm characteristic of β -sheet secondary structures. The Fourier transform infrared (FTIR) spectrum of aggregated HET-s(218–289) was determined (Figure 5B). The amide I' band is made of three components, as seen in the second derivative spectrum (Figure 5B). The bands at 1625 and 1690/cm are assigned to antiparallel β -strands, and the band at 1670/cm is attributed to turns. In contrast to

full-length HET-s that kept a significant amount of native-like secondary structures after formation of amyloid fibrils (Dos Reis *et al.*, 2002), most if not all of HET-s(218–289) is converted into the cross β -sheet structure of the amyloid fibrils.

We conclude that the HET-s(218–289) peptide forms amyloid fibers *in vitro*. This peptide undergoes a transition from an essentially unordered state to a β -sheet-rich aggregated state.

A HET-s(218–289)–GFP fusion protein aggregates *in vivo* and propagates [Het-s]

To correlate the ability to form amyloid aggregates *in vitro* and prion propagation *in vivo*, we expressed the HET-s(218–289) peptide as a GFP fusion protein in *P. anserina*. HET-s(218–289) with a C-terminal GFP fusion was expressed under control of the strong constitutive GPD promoter from *Aspergillus nidulans* (Punt *et al.*, 1988). The pGPD-het-s(218–289)–GFP construct was introduced into a Δ *het-s* strain in which

the *het-s* locus was inactivated by gene replacement (Turcq et al., 1991). The transformants were then analyzed by fluorescence microscopy. About 40% of the transformants displayed diffuse fluorescence signals, while the remaining 60% displayed dot-like fluorescence signals (Table I). After contact with a wild-type [Het-s] strain, transformants displaying diffuse fluorescence also acquire dot-like GFP fluorescence (Figure 6A). All strains displaying dot-like GFP fluorescence were able to convert wild-type [Het-s*] strains to the [Het-s] phenotype (Table I). The same construct was also introduced in a wild-type *het-s* strain, thus already containing [Het-s]. In this case, all transformants spontaneously displayed dot-like GFP fluorescence (not shown).

A plasmid allowing expression of the same peptide without the GFP tag was constructed and introduced into the Δ *het-s* background. Out of 24 tested transformants, none was able to convert a [Het-s*] strain to the [Het-s] phenotype. The lack of detectable activity of this construct might be due to rapid degradation of the peptide when expressed in *P.anserina* cells. Consistent with this hypothesis is the fact that the HET-s(218–289) peptide could not be detected in crude *P.anserina* cell extracts by western blot, whereas the HET-s(218–289)–GFP fusion protein was readily detected (data not shown).

We conclude that the peptide encompassing residues 218–289 can propagate [Het-s] *in vivo* at least when fused to the GFP.

A deletion of the C-terminal region of HET-s prevents *in vitro* aggregation

We next constructed a vector allowing expression in *E.coli* of a HET-s protein deleted of the C-terminal proposed amyloid-forming domain. For experimental convenience, the first deletion construct spanned residues 1–227, and thus corresponds to a deletion of the 62 C-terminal residues. The histidine-tagged HET-s(1–227) protein was

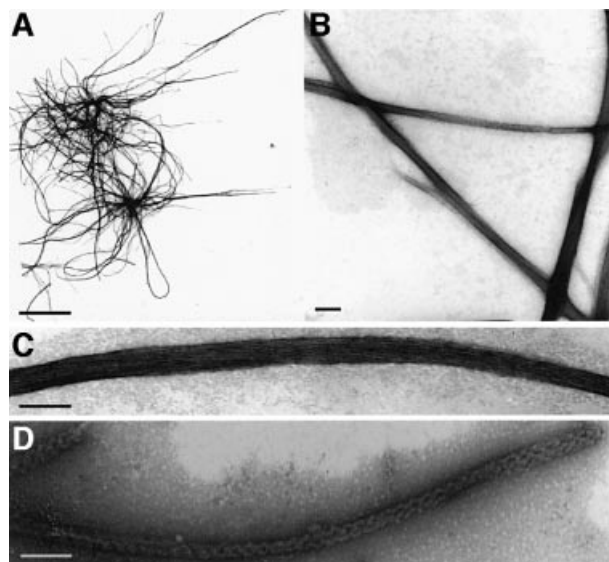


Fig. 3. Electron micrographs of HET-s(218–289) fibers. (A–C) Negatively stained electron fibers of HET-s(218–289). (D) Negatively stained full-length HET-s fibers. Scale bar = 5 μ m in (A) and 50 nm in (B–D).

expressed as a soluble protein in *E.coli* and purified under non-denaturing conditions. The HET-s(1–227) protein remains soluble upon prolonged storage and does not precipitate when inoculated with amyloid aggregates of full-length HET-s or HET-s(218–289) (Figure 4C). The protein is well folded as judged by near UV CD spectroscopy (not shown). The far UV CD spectrum indicates a mainly α -helical secondary structure content with two characteristic minima at 208 and 222 nm (Figure 5C). We compared the CD spectrum of HET-s(1–227) with that of full-length HET-s. The difference spectrum shows a minimum at 198 nm, suggesting a higher content in random coil secondary structure in HET-s compared with HET-s(1–227). The C-terminal region of HET-s appears to be unstructured in full-length HET-s, as it is when expressed as an isolated peptide.

Together, these data suggest that the region spanning residues 1–227 forms a globular domain representing an independent folding unit and confirm that the C-terminal region of HET-s is required for amyloid formation *in vitro*.

We also constructed a vector allowing expression of the region spanning residues 1–217, thus missing exactly the region identified as protected from proteolysis in the amyloid state of HET-s. This protein formed inclusion bodies when produced in *E.coli* and was purified under denaturing conditions. The protein could not be refolded

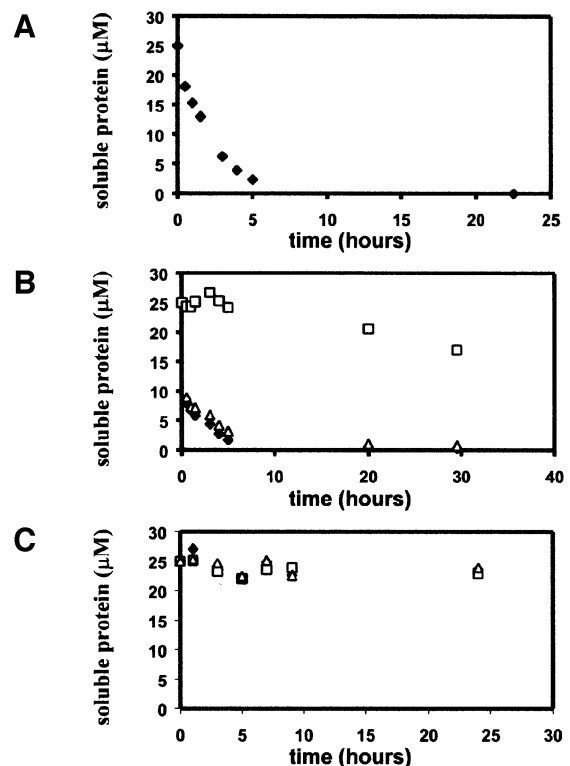


Fig. 4. Time course of aggregation of HET-s(218–289) and lack of aggregation of HET-s(1–227). (A) Time course of HET-s(218–289) aggregation at 25 μ M at pH 8 and 25°C. (B) Aggregation of recombinant HET-s protein at 25 μ M inoculated with 2.5 μ M aggregated HET-s (triangles), aggregated HET-s(218–289) (filled diamonds) or buffer alone (squares). (C) Lack of aggregation of recombinant HET-s(1–227) at 25 μ M inoculated with 2.5 μ M aggregated HET-s (triangles), aggregated HET-s(218–289) (filled diamonds) or buffer alone (squares).

properly; in non-denaturing buffer conditions, the protein displayed characteristics of a molten globule (S.Dos Reis and I.Lascu, unpublished data). These results suggest that

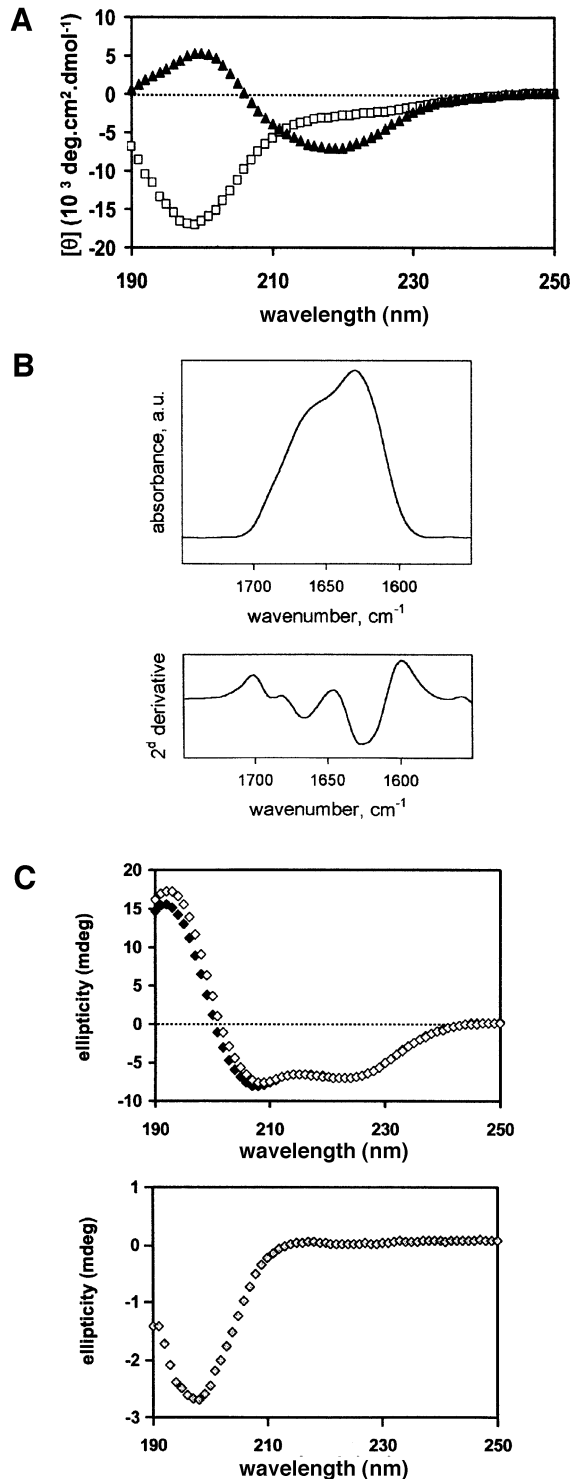


Fig. 5. CD and infrared spectra of HET-s(218–289) and HET-s(1–227). (A) CD spectrum of recombinant HET-s(218–289) at 25 μ M at pH 8 in the soluble (squares) and aggregated state (triangles). (B) FTIR spectrum of aggregated HET-s(218–289). The raw spectrum and the second derivative of the spectrum are given. (C) CD spectra of HET-s (filled diamonds) and HET-s(1–227) (open diamonds) at 2 μ M protein. The lower panel is the difference spectrum between HET-s and HET-s(1–227).

a region from residues 218 to 227 might be required for proper folding of the N-terminal globular domain of HET-s. Consistent with this hypothesis, is the fact that secondary structure prediction programs propose the existence of an α -helix spanning residues 208–223 (Figure 1).

For further analyses, we thus chose to study the HET-s(1–227) protein.

HET-s(1–227) fails to propagate [Het-s] and remains soluble *in vivo*

The HET-s(1–227) protein was expressed in *P.anserina* either alone or as a C-terminal GFP fusion. The HET-s(1–227) constructs were expressed under control of the GPD promoter and introduced into a Δ *het-s* recipient. Out of 24 tested transformants, none was able to convert a [Het-s*] to the [Het-s] state (Table I). In all analyzed transformants, GFP fluorescence was diffuse and cytoplasmic, both before and after contact with wild-type [Het-s] (Figure 6B). The constructs were also introduced into the wild-type *het-s* background. No GFP aggregation was detected. Therefore, even in the presence of the prion form of full-length HET-s, no aggregation of HET-s(1–227)–GFP took place. Such transformants still expressed the [Het-s] phenotype (Table I). Overexpression of the N-terminal domain of HET-s apparently did not affect endogenous [Het-s].

We conclude that the 62 C-terminal amino acids of HET-s are required for [Het-s] propagation and *in vivo* aggregation of HET-s.

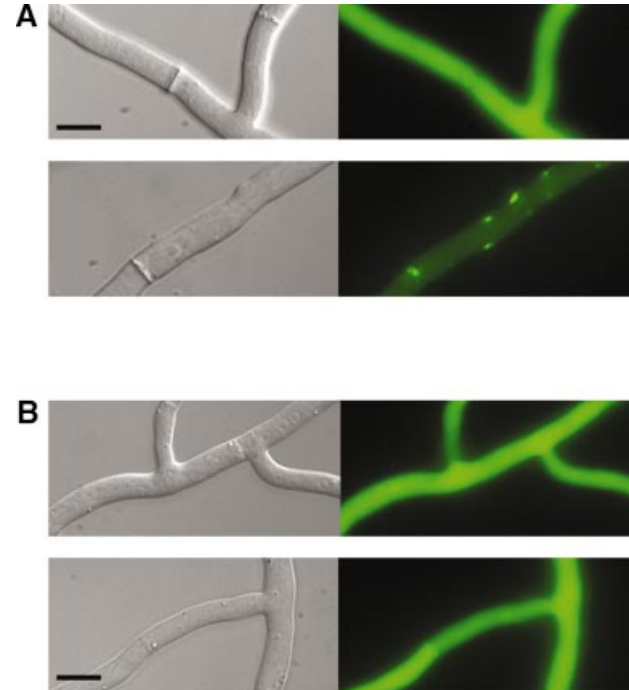


Fig. 6. *In vivo* distribution of HET-s(218–289)–GFP and HET-s(1–227) fusion proteins. (A) Fluorescence in a Δ *het-s* strain expressing HET-s(218–289)–GFP fusion protein, before (upper panel) and after (lower panel) contact with a [Het-s] strain. Scale bar = 5 μ m. (B) GFP fluorescence in a Δ *het-s* strain expressing a HET-s(1–227)–GFP fusion protein, before (upper panel) and after (lower panel) contact with a [Het-s] strain. Scale bar = 5 μ m.

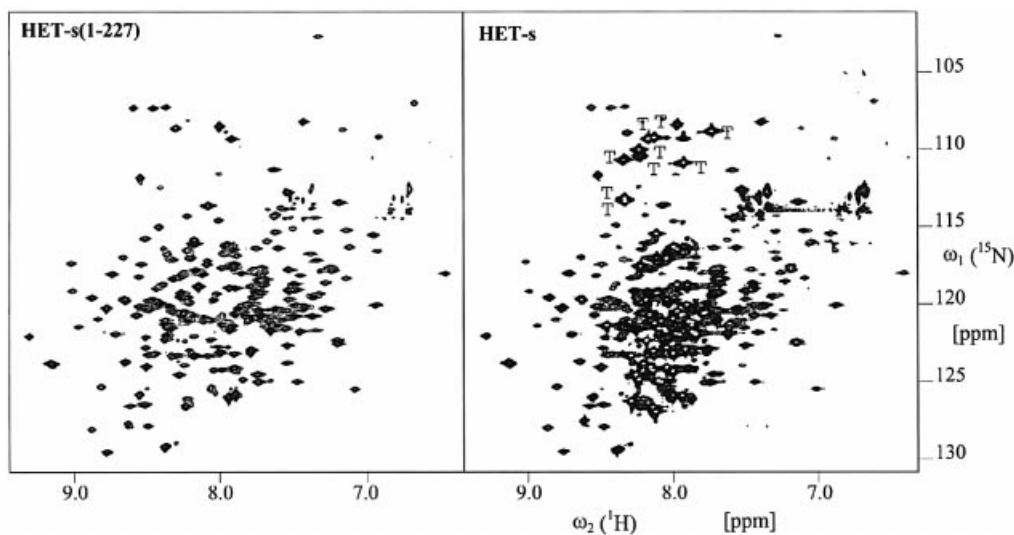


Fig. 7. Two-dimensional $[^{15}\text{N}, ^1\text{H}]$ -TROSY spectra of $\sim 60\%$ ^2H -, ^{15}N -labeled HET-s(1–227) and HET-s and corresponding cross-sections of HET-s as indicated in the two-dimensional spectrum. Designated with ‘T’ are the cross-peaks observed only for HET-s and located in the regions of ^{15}N - ^1H moieties of glycines. The N–H moieties of the side chains are largely suppressed due to the use of TROSY. Some additional sharp cross-peaks of low intensity can be observed that probably reflect a minor contamination with proteolytic degradation products of HET-s.

NMR analyses of HET-s and HET-s(1–227) reveal a C-terminal flexible domain

The data obtained so far suggest that HET-s comprises an N-terminal, mainly α -helical, folded domain and a C-terminal unordered domain. We further characterized HET-s using multi-probe nuclear magnetic resonance (NMR) spectroscopy to elucidate the domain structure of HET-s. In the $[^{15}\text{N}, ^1\text{H}]$ -TROSY spectrum of HET-s (Figure 7), two qualitatively different kinds of peaks can be distinguished, i.e. a first group of ~ 220 broad cross-peaks with full line widths at half-height along $\omega_2(^1\text{H})$ of ~ 25 Hz, and a second group of sharp, more intense peaks with line widths of ~ 14 Hz. These sharp and intense peaks are indicative of amino acid residues in a flexible conformation. Comparison with the $[^{15}\text{N}, ^1\text{H}]$ -TROSY spectrum of HET-s(1–227) (Figure 7) shows that the positions of the broad peaks in the intact protein coincide very closely with the peaks of HET-s(1–227) and that almost all the cross-peaks observed in HET-s(1–227) have their counterpart in HET-s. Missing broad peaks may not have been identified due to overlap with high-intensity peaks. A count of the remaining peaks revealed ~ 58 additional peaks that belong to the group of sharp and more intense peaks. These peaks are located in the ‘random coil’ region of the amide hydrogens between 7.85 and 8.46 p.p.m.. This group of 58 sharp and intense cross-peaks accounts well for the total number of 62 amide groups in the polypeptide segment 228–289. For example, the polypeptide segment 228–289 contains nine glycines, and in the glycine region of the $[^{15}\text{N}, ^1\text{H}]$ -TROSY spectrum of HET-s we count nine additional sharp and intense cross-peaks when compared with the spectrum of HET-s(1–227). There is a single tryptophan (W²⁸⁷) in the segment 228–289, and indeed one additional intense sharp cross-peak located in the indole region is observed in the $[^{15}\text{N}, ^1\text{H}]$ -TROSY spectrum of HET-s (data not shown). The observation that all cross-peaks attributed to residues 228–289 are sharp and intense and that these

cross-peaks are located in the ‘random coil’ chemical shift region of the amide hydrogens strongly supports the proposition of a flexible C-terminal tail corresponding to residues 228–289. For a further validation of the flexibility of the C-terminal 62 residues, $^{15}\text{N}\{^1\text{H}\}$ -nuclear Overhauser effects (NOEs) were recorded at a ^1H frequency of 700 MHz (Figure 8). Here, one expects peaks with a positive sign and relative intensity of 0.7–1 for ^{15}N - ^1H groups located in a folded protein domain (effective rotational correlation times $\tau_c \gg 2$ ns), and peaks with a negative sign or very small positive values for flexibly disordered ^{15}N - ^1H groups (τ_c values < 2 ns). Indeed, all the cross-peaks attributed to residues 228–289 show ^{15}N -NOEs close to zero (< 0.3), indicating high flexibility (Figure 8). In summary, it can be concluded on the basis of the reported NMR data that residues 228–289 are flexibly disordered, whereas the construct HET-s(1–227) consists of a globular domain which is preserved in full-length HET-s.

Limited proteolysis of soluble HET-s

Limited proteolysis can be used to probe the domain structure of proteins (Hubbard, 1998). We have reported that the proteinase K digestion patterns of the soluble and aggregated forms of HET-s differ considerably (Dos Reis *et al.*, 2002). A fragment of ~ 25 kDa was detected specifically for the soluble form, but only at short digestion times. These experiments were designed to provide evidence for resistance of the amyloid core and thus used a high enzyme to substrate ratio ($\sim 1:50$). We repeated these experiments using much lower amounts of proteinase K ($\sim 1:5000$ enzyme to substrate ratio). The partial digestion products of soluble HET-s migrate as a single band of ~ 25 kDa on SDS-PAGE (Figure 2B). This band appears after short digestion times and remains stable upon prolonged exposure to proteinase K. We have analyzed these digestion products by mass spectrometry and Edman N-terminal sequencing. The same analysis of full-length

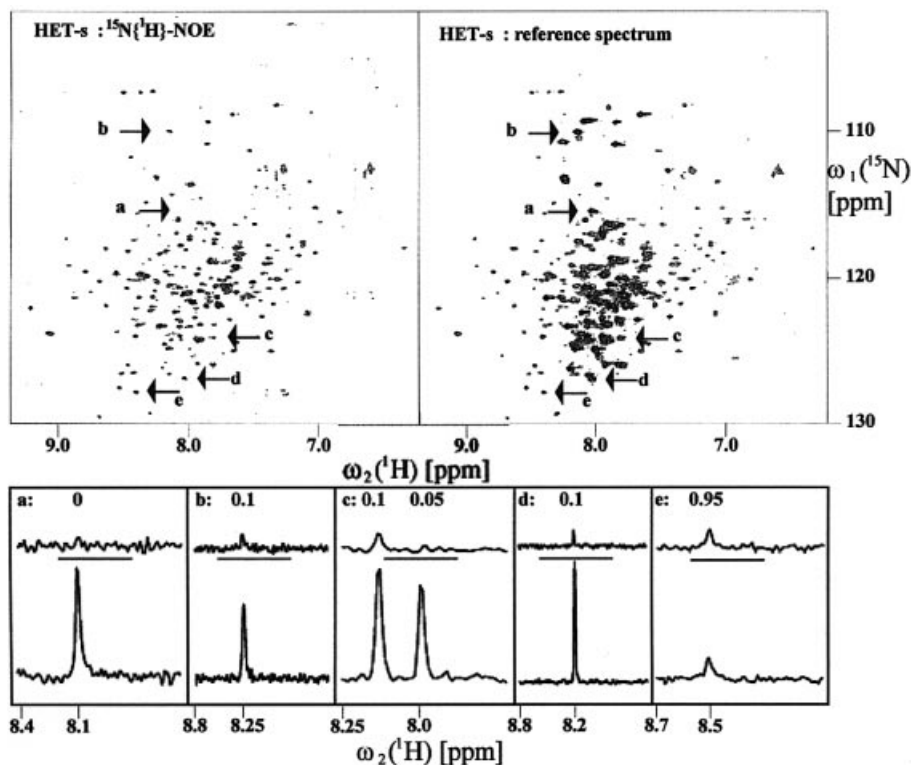


Fig. 8. Two-dimensional $^{15}\text{N}\{^1\text{H}\}$ -NOE spectrum and the corresponding reference spectrum of $\sim 60\%$ ^2H -, ^{15}N -labeled HET-s. In addition, selected cross-sections of cross-peaks assigned to residues 228–289 (a–d) and one cross-peak assigned to residues 1–227 (e) are shown. For these chosen cross-peaks, $^{15}\text{N}\{^1\text{H}\}$ -NOE values derived from the ratio between the intensity of the cross-peak of the $^{15}\text{N}\{^1\text{H}\}$ -NOE spectrum and the reference spectrum are given.

HET-s indicated that the recombinant protein had undergone excision of the initiator methionine, as expected from the occurrence of a serine as the penultimate residue (Hirel *et al.*, 1989). The analysis of proteinase K-resistant products revealed the presence of two peptides comprising residues 2–240 and 10–240 (Table II). In a sample corresponding to the longer digestion time (3 h), the smaller form (10–240) was more abundant than after a short digestion time (1.5 h), suggesting that the smaller form derived from further proteolysis of the larger one. To confirm that in both products the C-terminal residue was Q^{240} , we performed a complete digestion of both the full-length HET-s protein and the proteinase K-treated sample with Asp-N protease and analyzed the digestion products by mass spectrometry. As residue 230 is the first aspartate found upstream of position 240, a 230–240 peptide is expected among the Asp-N digestion products of the proteinase K-treated sample. We identified a peptide with the expected molecular weight (1372.74 Da), and the PSD fragmentation of this ion confirmed the $^{230}\text{DIRTEERARVQ}^{240}$ sequence (Table II). This 230–240 peptide was not detected among the Asp-N digestion products of full-length HET-s.

We conclude that limited proteolysis of soluble HET-s generates mainly two peptides: 2–240 and 10–240. These experiments confirm the existence of an N-terminal well-folded globular domain in HET-s and show that, in sharp contrast to the amyloid form, the C-terminal region in soluble HET-s is highly sensitive to proteolysis.

We have expressed the HET-s protein truncated at position 240 in *P.anserina*. Like HET-s(1–227), this construct was unable to propagate [Het-s] *in vivo* (Table I). A HET-s(1–240)–GFP fusion protein had a diffuse cytoplasmic distribution (not shown). Recombinant HET-s(1–240) was expressed as a soluble protein in *E.coli* and remained soluble *in vitro* even when inoculated with aggregated HET-s (not shown).

The prion-forming domain and the incompatibility function

In order to determine the involvement of the prion-forming domain in the [Het-s]-associated cell death reaction, we analyzed the strains expressing the different HET-s deletion constructs for their incompatibility function. The incompatibility function is assayed by confronting strains on solid medium. If the strains are incompatible, the cell death reaction occurring in the confrontation margin leads to the formation of an abnormal contact line termed a barrage. Out of 24 tested HET-s(1–227) or HET-s(1–227)–GFP transformants, none produced a barrage reaction to the *het-S* tester, thus indicating that deletion of the C-terminal domain abolished the incompatibility function (Table I). Similarly, among the transformants expressing HET-s(1–240) or HET-s(1–240)–GFP, none produced a barrage reaction toward *het-S*. None of the HET-s(218–289) transformants produced a barrage reaction to *het-S*. As discussed above, this might be attributed to the fact that HET-s(218–289) is

unstable and does not accumulate. Transformants expressing the HET-s(218–289)–GFP fusion did not produce a typical strong barrage reaction towards the *het-S* tester. However, they displayed an attenuated barrage reaction, suggesting that the construct retained part of the incompatibility activity. To analyze that point further, we have introduced the HET-s(218–289)–GFP construct into a *het-S* background. If the construct retained some incompatibility function, such transformants should display an altered growth phenotype. A fraction of the transformants displayed an altered growth phenotype, again suggesting that part of the incompatibility function had been retained (not shown). The growth alteration was not as strong as the one observed when wild-type HET-s is expressed in a *het-S* background.

We conclude that the C-terminal domain of HET-s is necessary for the incompatibility function. However, it is not sufficient *per se* to produce a full incompatibility reaction towards *het-S*.

In order also to analyze the role of the C-terminal domain in the incompatibility function of the non-prion HET-S variant, we deleted the C-terminal domain of HET-S. The plasmid allowing expression of HET-S(1–227) was introduced into the Δ *het-s* deletion strain. Transformants expressing HET-S(1–227) failed to produce a barrage reaction to [Het-s] strains (Table I). We conclude that the C-terminal domain is also required for the incompatibility function of the HET-S variant.

The N-terminal region of HET-S inhibits transition to the prion state

The HET-S protein differs from HET-s by 13 amino acid differences (10 in the N-terminal domain and three in the C-terminal flexible domain) but lacks the prion behavior (Figure 1). We constructed chimeric alleles between *het-s* and *het-S* by exchanging the regions coding for the C- and N-terminal domains. The *het-sS* construct allows expression of the globular domain of HET-s fused to the C-terminal domain of HET-S while, reciprocally, the *het-Ss* construct allows expression of the N-terminal domain of HET-S fused to the C-terminal flexible domain of HET-s. The corresponding constructs were introduced into a Δ *het-s* strain and the transformants were tested for their incompatibility phenotype and for the ability to induce the appearance of the [Het-s] phenotype in a [Het-s*] strain. Transformants expressing the *het-sS* chimeric allele display the [Het-s] phenotype. After being confronted with a wild-type [Het-s] strain, they produce a barrage reaction to a *het-S* tester and are able to convert a [Het-s*] strain to the [Het-s] phenotype (Table I). Conversely, transformants expressing *het-Ss* display the [Het-S] phenotype. Namely, they produce a barrage reaction to a [Het-s] tester and are unable to convert a [Het-s*] strain to the [Het-s] phenotype even after being confronted with a wild-type [Het-s] strain. As expected, *het-sS* transformants were incompatible with *het-Ss* transformants. These chimeric alleles were also expressed using the strong GPD promoter, yielding the same observations. Together, these results show that the C-terminal domain of HET-S can substitute for the C-terminal domain of HET-s. Conversely, the prion-forming domain of HET-s is unable to propagate [Het-s] when fused to the N-terminal domain of HET-S. In other

words, the globular domain of HET-S exerts an inhibitory effect *in cis* on the transition to the prion state. Expression of HET-S(1–227) in a wild-type [Het-s] strain did not alter expression of the [Het-s] phenotype of the recipient, suggesting that this inhibitory effect does not occur *in trans*.

These experiments also indicate that the incompatibility type ([Het-s] or [Het-S]) is specified by the N-terminal domain.

Discussion

The HET-s protein is a fungal prion involved in a genetically controlled cell death mechanism. Previous analyses have connected [Het-s] prion propagation to amyloid formation. The present work now documents the domain structure–function relationship of the HET-s protein.

Domain organization of HET-s

We show herein that HET-s comprises an N-terminal folded, mainly α -helical, globular domain and a C-terminal flexible domain responsible for prion propagation and amyloid formation. The structural definition of both domains was based on a number of different experimental approaches that gave globally concordant results. The NMR experiments identify 58 additional peaks corresponding to unordered residues in the spectrum of full-length HET-s compared with HET-s(1–227). This suggests that the structured region ends around residue 230. The proteolysis-resistant domain of soluble HET-s spans to residue 240. Thus the definition of the globular domain provided by these two methods differs somewhat. Still, importantly, both the NMR data and the limited proteolysis experiments suggest that the structured part of HET-s extends past residue 217. This assumption is supported by the observation that HET-s(1–217), in contrast to HET-s(1–227), does not fold properly. We therefore propose that the globular domain of HET-s extends past residue 218 and approximately down to residue 230, and that a C-terminal region of ~60 residues is flexibly disordered. On the basis of limited proteolysis experiments of the aggregated form of HET-s, we show that the amyloid core of HET-s starts at residue 218. Thus, upon aggregation, the flexible C-terminal domain of HET-s undergoes a transition from an essentially unordered to an amyloid β -sheet-rich structure. Since the structured domain is proposed to extend past residue 217, it appears that a short region in the C-terminal end of the structured domain (218 to ~230) is also incorporated into the amyloid core. EM revealed marked differences between HET-s(218–289) and full-length HET-s fibers. The HET-s(218–289) fibers are smooth and associate laterally into well-ordered bundles, while full-length HET-s fibrils are twisted and rugged. This difference presumably is due to the fact that the globular domain imposes spatial constraints to be fitted into the aggregate.

Structural flexibility as a common feature of prion proteins

We document that the prion-forming domain is unstructured in solution when expressed alone, and our NMR data provide direct evidence that the C-terminal region is

flexibly disordered in the soluble form of the full-length protein. HET-s shares the described two-domain organization with the two yeast prion model proteins Ure2p and Sup35p and the mammalian prion proteins. Both Ure2p and Sup35p proteins display a C-terminal folded domain and an N-terminal prion-forming domain (PFD) which is proposed to be unstructured (Perrett *et al.*, 1999; Scheibel and Lindquist, 2001; Thual *et al.*, 2001). The yeast prion-forming domains of Ure2p and Sup35p are characterized by a biased amino acid composition. Both domains are N and Q rich. High N/Q content is a general characteristic of the yeast prion domains (reviewed in Tuite, 2000). The prion-forming domain of HET-s is not N/Q rich. Except for a relatively high glycine content (14%), the amyloid-forming domain of HET-s does not display any obvious composition bias or repeat structure.

Recombinant PrP also displays a highly flexible N-terminal domain spanning residues 23–120 (Riek *et al.*, 1997; Wuthrich and Riek, 2001). This sequence fragment is critical for prion infectivity: although the lack of residues 23–93 does not abolish prion infectivity, prion propagation experiments with shorter constructs were not successful (Fischer *et al.*, 1996; Flechsig *et al.*, 2000), deletions within the sequence fragment 23–120 influence the efficiency of prion propagation (Flechsig *et al.*, 2000; Supattapone *et al.*, 2001), expansion of the unstructured region by a number of octapeptide repeats was found to be associated with a number of cases of inherited Creutzfeldt–Jakob disease, and three point mutations (P102L, P105L and A117V) associated with familial prion disease are located within this fragment (reviewed in Weissmann, 1999). This argues for a role for this region in modulating prion infectivity.

The fact that all prion proteins identified so far present a folded globular domain attached to a highly flexible domain suggest strongly that this domain organization is a relevant feature for generation of prion infectivity. However, despite this observed consensus structural motif, further similarities between the yeast, *P.anserina* and mammalian prion proteins are not obvious: (i) the prion-forming domains share no universal sequence homology; and (ii) the fungal flexible prion domains can support infectivity without the structured domain, whereas in the case of mammalian PrP, both domains seem to be required for prion activity.

Role of the globular domain in the control of prion propagation

Our data indicate that the C-terminal domain adopts an unordered structure both as an isolated peptide and when attached to the globular domain. Therefore, at least in the tested conditions, the N-terminal globular domain does not appear to organize the flexible C-terminal region. Reciprocally, our NMR data indicate that the structure of the folded N-terminal domain is not affected by deletion of the C-terminal region. The N-terminal domain can fold independently of the flexible C-terminal domain. These results suggest that the interactions between the two domains are relatively modest. However, the construction of chimeric proteins between HET-s and the HET-S non-prion variant uncovered important functional interactions between the two domains. In fact, we show that the lack of prion behavior for HET-S is due to the inhibitory effect of

the N-terminal folded domain rather than being due to polymorphism in the amyloid-forming domain. Consistent with this hypothesis is the observation that the HET-S(218–289) peptide forms amyloid fibrils *in vitro* (S.Dos Reis, unpublished data). The functional importance of the N-terminal domain was already suggested by previous genetic analyses showing that the non-prion HET-S variant can be converted to an active prion form by point mutations in the N-terminal domain (Deleu *et al.*, 1993). For instance, a HET-S H33P mutant protein behaves as HET-s *in vivo*. One can envisage two main hypotheses to explain how the globular domain of HET-S can inhibit prion formation. First, in HET-S, the C-terminal domain might interact with the N-terminal globular domain and therefore be less flexible, and consequently less prone to aggregation. Also, it is possible, as proposed in the case of numerous amyloidogenic proteins, that partially unfolded species of HET-s are the template for aggregation. Then, if the globular domain of HET-s is destabilized compared with HET-S, *in vivo* prion formation might only be possible for HET-s. Comparison of the structural properties of HET-s and HET-S will allow that point to be addressed in the future.

Does the globular domain retain its native fold in the fibrils?

Our data document the conformational transition occurring in the flexible C-terminal domain of HET-s. It remains to be established whether folding of the N-terminal globular domain is affected upon aggregation or if it retains its native fold. In a simple model, acquisition of the infectious [Het-s] state could be understood as a conformational transition involving only the unstructured C-terminal domain. In the case of Ure2p, the globular domain of the protein apparently retains its native fold in the aggregated state of the protein (Bousset *et al.*, 2002). Moreover, it was shown that numerous enzymes retain their activity when fused to the PFD of Ure2p and incorporated into fibrils (Baxa *et al.*, 2002). In the case of HET-s, CD and FTIR analyses suggest that in addition to an increase in the β -sheet content, aggregation is correlated with a decrease in α -helicity (Dos Reis *et al.*, 2002). Moreover, the N-terminal region of HET-s appears to be more sensitive to proteolysis in the aggregated state than in the soluble form (S.Dos Reis, unpublished data). Both observations suggest that the structure of the globular domain of HET-s might be affected upon amyloid formation. As discussed above, we propose that the folded domain of HET-s extends past residue 217 and that the region from residue 218 to ~230 might participate in the overall stability of the globular domain. Sequestration of that region in the amyloid core might thus destabilize the globular domain of HET-s and thus lead to its unfolding upon aggregation of the C-terminal domain.

Amyloid aggregation and the incompatibility function

Deletion of the HET-s domain required for amyloid formation abolishes the incompatibility function, i.e. the [Het-s]-associated cell death reaction. This result suggests that the cell death reaction occurring in mixed *het-s/het-S* cells is intimately linked to amyloid formation. Deletion of that same region in the antagonistic non-prion HET-S

variant also abolishes its incompatibility function, further emphasizing the importance of that region in the control of the cell death reaction. Toxicity of the HET-s–HET-S interaction can be explained in the following model. We show here that the C-terminal domains of HET-s and HET-S are functionally equivalent. It is therefore very likely that the HET-S C-terminal domain can interact with the C-terminal domain of HET-s. Incorporation of a HET-S monomer into the HET-s aggregate would ‘poison’ it and prevent further size increase of the aggregate, possibly because the globular domain of HET-S cannot be incorporated into HET-s aggregates. Accumulation of oligomeric HET-s species halted in their aggregation process would be toxic to the cell, while fully assembled HET-s fibrils would be innocuous. Our present understanding of the domain organization of HET-s now leads us to design experiments that will allow the analysis of the mechanism of toxicity of the HET-s–HET-S interaction. This dissection in a tractable microorganism might be relevant to the understanding of prion diseases and human amyloid pathologies in general.

Materials and methods

Detailed information on the plasmid construction, the microscopy methods, N-terminal sequencing and mass spectrometry are provided as Supplementary data available at *The EMBO Journal* Online.

Podospora methods

Three *P. anserina* strains were used in this study, the *het-S* strain, the *het-s* strain, and the Δ *het-s* strain in which the *het-s* gene has been disrupted by gene replacement (Turcq *et al.*, 1991). In this strain, the promoter region and the 5' part of the *het-s* gene have been deleted and replaced by the *ura5* marker. All strains were isogenic except for the *het-s* locus. The [Het-s*] strains were obtained as the progeny of a *het-S* × *het-s* cross.

Incompatibility phenotypes were determined by performing barrage tests on corn meal agar medium as previously described (Maddelin *et al.*, 2002). The ability to convert a [Het-s*] strain to [Het-s] was assayed as described (Maddelin *et al.*, 2002) except that strains were subcultured twice before assaying their [Het-s] phenotype. DNA-mediated transformation of *Podospora* strains was performed as described (Bergès and Barreau, 1989). Plasmids were introduced in co-transformation experiments using a 10:1 molar ratio between the plasmid of interest and the pCB1004 vector carrying the *hygR* gene used as selective marker (Carroll *et al.*, 1994). Transforming DNA integrates in the genome mainly by non-homologous recombination, therefore all transformants display a distinct genetic constitution. Thus, in each experiment, from 12 to 24 individual transformants were analyzed.

Protein expression and purification

The histidine-tagged HET-s(218–289) peptide was expressed and purified from inclusion bodies under denaturing conditions as previously described for full-length HET-s (Dos Reis *et al.*, 2002). This yields ~2–4 mg of peptide per liter of culture. The peptide was pure as judged by SDS–PAGE followed by Coomassie Blue staining. To eliminate urea, the peptide was then submitted to gel filtration on Sephadex G-25, using 175 mM acetic acid as an eluent. Subsequently, the pH was brought to 8 by adding 90 μ l of 2 M Tris base per ml.

For expression and purification of stable isotope-labeled HET-s and HET-s(1–227), 2 l of LB medium were inoculated with an overnight culture of BL21(DE3) bearing the plasmid to be expressed. At an OD₆₀₀ of 0.8–1.0, cells were pelleted by a 10 min centrifugation at 4000 g. The cells were washed using an M9 salt solution, excluding all nitrogen sources. In order to generate ~60% ²H-, uniformly ¹⁵N-labeled protein, the cell pellet was resuspended in 0.5 l of minimal medium using D₂O (>97%, Spectra Isotopes) as solvent and ¹⁵N-labeled ammonium sulfate as the sole nitrogen source. After 2 h of adjustment to the new medium, the bacteria were induced with isopropyl-1-thio- β -D-galactopyranoside (1 mM) for 6 h at 37°C. HET-s was purified as described previously (Dos Reis *et al.*, 2002). This procedure yielded 35–40 mg of 60% ²H-, uniformly ¹⁵N-labeled HET-s. The HET-s protein behaves well at pH 7.0

at 30°C in 95% H₂O/5% ²H₂O containing 100 mM sodium phosphate buffer and a protein concentration of ~1 mM for several days until it starts to aggregate slowly into amyloid fibrils.

HET-s(1–227) did not form inclusion bodies. The cell pellet was therefore solubilized and sonicated in 100 mM Tris pH 8.0, 300 mM NaCl, the lysate centrifuged for 30 min at 12 000 g and the supernatant directly applied to His₆ affinity chromatography. The protein was dialyzed exhaustively against 50 mM sodium phosphate pH 7.5 and then once against 50 mM sodium phosphate pH 7.0, 1 mM dithiothreitol (DTT). After concentrating the sample, the DTT concentration was adjusted to 5 mM. This procedure yielded 35–40 mg of ~60% ²H-, uniformly ¹⁵N-labeled HET-s(1–227). The HET-s(1–227) construct behaves well for several weeks at pH 7.0 at 30°C in 95% H₂O/5% ²H₂O containing 100 mM sodium phosphate buffer and 5 mM DTT, and a protein concentration of 2 mM.

NMR

NMR experiments were carried out either with ~60% ²H-, uniformly ¹⁵N-labeled HET-s(1–227) or HET-s. The measurements were performed at 700 MHz ¹H frequency on a Bruker Avance spectrometer equipped with five radio-frequency channels, a pulsed-field gradient unit and a triple resonance probe with an actively shielded z-gradient coil. Measurements were performed at 30°C and pH 7.0 in 95% H₂O/5% D₂O containing 100 mM sodium phosphate, 5 mM DTT and a protein concentration of 2 mM for HET-s(1–227) or 0.8 mM for HET-s. The following parameter settings were used for the [¹⁵N, ¹H]-TROSY experiments (Pervushin *et al.*, 1997): data size 350(*t*₁) × 1024(*t*₃) complex points; *t*_{1,max} (¹⁵N) = 150 ms, *t*_{2,max} (¹H) = 75.6 ms, respectively. The data set were zero-filled to 1024 × 2048 complex points; 16 scans per increment were acquired. Prior to Fourier transformation, the data were multiplied with a 75° shifted sine bell window in both dimensions. 15N{¹H}-NOEs were measured using the procedure described by Zhu *et al.* (2000) with a relaxation delay of 3 s and a proton saturation length of 3 s achieved by applying a train of 120° pulses at 20 ms intervals. The data set was recorded with a data size 150(*t*₁) × 1024(*t*₃) complex points; *t*_{1,max} (¹⁵N) = 50 ms, *t*_{2,max} (¹H) = 75.6 ms. The data sets were zero-filled to 1024 × 2048 complex points; 64 scans per increment were acquired. Prior to Fourier transformation, the data were multiplied with a 75° shifted sine bell window in both dimensions.

Spontaneous and seeded aggregation assays

Protein solutions were incubated at room temperature in 50 mM Tris pH 8.0, 150 mM NaCl. Protein precipitation was analyzed at various time points by centrifuging 50 μ l aliquots for 15 min at 10 000 g. Supernatant and pellet fractions were analyzed by SDS–PAGE followed by Coomassie Blue staining, and the protein concentration in the supernatant fractions was measured using the BioRad protein assay reagent and determining absorbance at 280 nm. For seeding assays, a protein solution in 50 mM Tris pH 8.0, 150 mM NaCl at 25 μ M was inoculated with 2.5 μ M aggregated protein. The aggregated protein sample was sonicated briefly prior to inoculation. Protein precipitation was analyzed as described above.

Circular dichroism and FTIR

CD spectra were recorded at 20°C using a Jasco 810 spectropolarimeter with a quartz cell of 0.1 cm path length.

FTIR spectra were recorded at 20°C using a JASCO FT/IR-610 spectrometer. Interferograms were acquired at 4/cm nominal resolution and are the average of 1000 scans. CaF₂ plates and a 100 μ m spacer were used. Protein concentration was 4 mg/ml. The sample was buffered at pH 8 using Tris–HCl. The software provided by JASCO Corporation with the spectrometer was used for the spectrum deconvolution (band width 30/cm) and for the fitting of the spectra by a sum of Lorentzians in order to estimate the secondary structure contents.

Limited proteolysis of HET-s with proteinase K

A 30 μ M solution of aggregated HET-s protein was treated for 1 h at 37°C with 20 μ g/ml of proteinase K in 50 mM Tris pH 8.0, 150 mM NaCl. For soluble HET-s, a 30 μ M solution of HET-s was treated with 0.2 μ g/ml of proteinase K at 25°C in 50 mM Tris pH 8.0, 150 mM NaCl for various times. Reactions were stopped by addition of 1 vol. of SDS–PAGE loading buffer and heated at 100°C for 5 min.

Supplementary data

Supplementary data are available at *The EMBO Journal* Online.

Acknowledgements

This research is supported by the GIS prion. A.B. is a recipient of a fellowship from the GIS prion. S.D.R. is a fellow of the Ministère de la Recherche et l'Enseignement Supérieur.

References

- Baxa,U., Speransky,V., Steven,A.C. and Wickner,R.B. (2002) Mechanism of inactivation on prion conversion of the *Saccharomyces cerevisiae* Ure2 protein. *Proc. Natl Acad. Sci. USA*, **99**, 5253–5260.
- Bergès,T. and Barreau,C. (1989) Heat-shock at elevated temperature improves transformation efficiency of protoplasts from *Podospora anserina*. *J. Gen. Microbiol.*, **135**, 601–604.
- Bousset,L., Thomson,N.H., Radford,S.E. and Melki,R. (2002) The yeast prion Ure2p retains its native α -helical conformation upon assembly into protein fibrils *in vitro*. *EMBO J.*, **21**, 2903–2911.
- Carrol,A.M., Sweigard,J.A. and Valent-Central,B. (1994) Improved vectors for selecting resistance to hygromycin. *Fungal Genet. Newslett.*, **41**, 22.
- Coustou,V., Deleu,C., Saupe,S. and Begueret,J. (1997) The protein product of the het-s heterokaryon incompatibility gene of the fungus *Podospora anserina* behaves as a prion analog. *Proc. Natl Acad. Sci. USA*, **94**, 9773–9778.
- Coustou-Linares,V., Maddelein,M.L., Bégueret,J. and Saupe,S.J. (2001) *In vivo* aggregation of the HET-s prion protein of the fungus *Podospora anserina*. *Mol. Microbiol.*, **42**, 1325–1335.
- Deleu,C., Clavé,C. and Bégueret,J. (1993) A single amino acid difference is sufficient to elicit vegetative incompatibility in the fungus *Podospora anserina*. *Genetics*, **135**, 45–52.
- Dobson,C.M. (1999) Protein misfolding, evolution and disease. *Trends Biochem. Sci.*, **24**, 329–332.
- Dos Reis,S., Couлары-Salin,B., Forge,V., Lascu,I., Bégueret,J. and Saupe,S.J. (2002) The HET-s prion protein of the filamentous fungus *Podospora anserina* aggregates *in vitro* into amyloid-like fibrils. *J. Biol. Chem.*, **277**, 5703–5706.
- Fischer,M., Rulicke,T., Raeber,A., Sailer,A., Moser,M., Oesch,B., Brandner,S., Aguzzi,A. and Weissmann,C. (1996) Prion protein (PrP) with amino-proximal deletions restoring susceptibility of PrP knockout mice to scrapie. *EMBO J.*, **15**, 1255–1264.
- Flechsigs,E., Shmerling,D., Hegyi,I., Raeber,A.J., Fischer,M., Cozzio,A., von Mering,C., Aguzzi,A. and Weissmann,C. (2000) Prion protein devoid of the octapeptide repeat region restores susceptibility to scrapie in PrP knockout mice. *Neuron*, **27**, 399–408.
- Glass,N.L., Jacobson,D.J. and Shiu,P.K. (2000) The genetics of hyphal fusion and vegetative incompatibility in filamentous ascomycete fungi. *Annu. Rev. Genet.*, **34**, 165–186.
- Glover,J.R., Kowal,A.S., Schirmer,E.C., Patino,M.M., Liu,J.J. and Lindquist,S. (1997) Self-seeded fibers formed by Sup35, the protein determinant of [PSI⁺], a heritable prion-like factor of *S.cerevisiae*. *Cell*, **89**, 811–819.
- Hirel,P.H., Schmitter,J.M., Dessen,P., Fayat,G. and Blanquet S. (1989) Extent of N-terminal methionine excision from *Escherichia coli* proteins is governed by the side-chain length of the penultimate amino acid. *Proc. Natl Acad. Sci. USA*, **86**, 8247–8251.
- Hubbard,S.J. (1998) The structural aspects of limited proteolysis of native proteins. *Biochim. Biophys. Acta*, **1382**, 191–206.
- King,C.Y., Tittmann,P., Gross,H., Gebert,R., Aebi,M. and Wuthrich,K. (1997) Prion-inducing domain 2–114 of yeast Sup35 protein transforms *in vitro* into amyloid-like filaments. *Proc. Natl Acad. Sci. USA*, **94**, 6618–6622.
- Koo,E.H., Lansbury,P.T., Jr and Kelly,J.W. (1999) Amyloid diseases: abnormal protein aggregation in neurodegeneration. *Proc. Natl Acad. Sci. USA*, **96**, 9989–9990.
- Maddelein,M.L., Dos Reis,S., Duvezin-Caubet,S., Couлары-Salin,B. and Saupe,S.J. (2002) Amyloid aggregates of the HET-s prion protein are infectious. *Proc. Natl Acad. Sci. USA*, **99**, 7402–7407.
- Perrett,S., Freeman,S.J., Butler,P.J. and Fersht,A.R. (1999) Equilibrium folding properties of the yeast prion protein determinant Ure2. *J. Mol. Biol.*, **290**, 331–345.
- Pervushin,K., Riek,R., Wider,G. and Wuthrich,K. (1997) Attenuated T2 relaxation by mutual cancellation of dipole–dipole coupling and chemical shift anisotropy indicates an avenue to NMR structures of very large biological macromolecules in solution. *Proc. Natl Acad. Sci. USA*, **94**, 12366–12371.
- Prusiner,S.B. (1998) Prions. *Proc. Natl Acad. Sci. USA*, **95**, 13363–13383.
- Punt,P.J., Dingemans,M.A., Jacobs-Meijnsing,B.J., Pouwels,P.H. and van den Hondel,C.A. (1988) Isolation and characterization of the glyceraldehyde-3-phosphate dehydrogenase gene of *Aspergillus nidulans*. *Gene*, **69**, 49–57.
- Riek,R., Hornemann,S., Wider,G., Glockshuber,R. and Wuthrich,K. (1997) NMR characterization of the full-length recombinant murine prion protein, mPrP(23–231). *FEBS Lett.*, **413**, 282–288.
- Roepstorff,P. and Fohlman,J. (1984) Proposal for a common nomenclature for sequence ions in mass spectra of peptides. *Biomed. Mass. Spectrom.*, **11**, 601.
- Saupe,S.J. (2000) Molecular genetics of heterokaryon incompatibility in filamentous ascomycetes. *Microbiol. Mol. Biol. Rev.*, **64**, 489–502.
- Scheibel,T. and Lindquist,S.L. (2001) The role of conformational flexibility in prion propagation and maintenance for Sup35p. *Nat. Struct. Biol.*, **8**, 958–962.
- Supattapone,S., Muramoto,T., Legname,G., Mehlhorn,I., Cohen,F.E., DeArmond,S.J., Prusiner,S.B. and Scott,M.R. (2001) Identification of two prion protein regions that modify scrapie incubation time. *J. Virol.*, **75**, 1408–1413.
- Taylor,K.L., Cheng,N., Williams,R.W., Steven,A.C. and Wickner,R.B. (1999) Prion domain initiation of amyloid formation *in vitro* from native Ure2p. *Science*, **283**, 1339–1343.
- Thual,C., Bousset,L., Komar,A.A., Walter,S., Buchner,J., Cullin,C. and Melki,R. (2001) Stability, folding, dimerization and assembly properties of the yeast prion Ure2p. *Biochemistry*, **40**, 1764–1773.
- Tuite,M.F. (2000) Yeast prions and their prion-forming domain. *Cell*, **100**, 289–292.
- Turcq,B., Deleu,C., Denayrolles,M. and Begueret,J. (1991) Two allelic genes responsible for vegetative incompatibility in the fungus *Podospora anserina* are not essential for cell viability. *Mol. Gen. Genet.*, **228**, 265–269.
- Weissmann,C. (1999) Molecular genetics of transmissible spongiform encephalopathies. *J. Biol. Chem.*, **274**, 3–6.
- Wickner,R.B. (1994) [URE3] as an altered URE2 protein: evidence for a prion analog in *Saccharomyces cerevisiae*. *Science*, **264**, 566–569.
- Wuthrich,K. and Riek,R. (2001) Three-dimensional structures of prion proteins. *Adv. Protein Chem.*, **57**, 55–82.
- Zhu,G., Xia,Y., Nicholson,L.K. and Sze,K.H. (2000) Protein dynamics measurements by TROSY-based NMR experiments. *J. Magn. Reson.*, **143**, 423–426.

Received February 3, 2003; revised March 10, 2003;
accepted March 11, 2003